

1 **MitoChime: A Machine-Learning Pipeline for**
2 **Detecting PCR-Induced Chimeras in**
3 **Mitochondrial Illumina Reads**

4 A Special Project Proposal
5 Presented to
6 the Faculty of the Division of Physical Sciences and Mathematics
7 College of Arts and Sciences
8 University of the Philippines Visayas
9 Miag-ao, Iloilo

10 In Partial Fulfillment
11 of the Requirements for the Degree of
12 Bachelor of Science in Computer Science

13 by

14 Duranne Duran
15 Yvonne Lin
16 Daniella Pailden

17 Adviser
18 Francis D. Dimzon, Ph.D.

19 December 5, 2025

Contents

21	1 Introduction	1
22	1.1 Overview	1
23	1.2 Problem Statement	3
24	1.3 Research Objectives	4
25	1.3.1 General Objective	4
26	1.3.2 Specific Objectives	4
27	1.4 Scope and Limitations of the Research	5
28	1.5 Significance of the Research	6
29	2 Review of Related Literature	7
30	2.1 The Mitochondrial Genome	7
31	2.1.1 Mitochondrial Genome Assembly	8

32	2.2 PCR Amplification and Chimera Formation	9
33	2.3 Existing Traditional Approaches for Chimera Detection	10
34	2.3.1 UCHIME	11
35	2.3.2 UCHIME2	12
36	2.3.3 CATch	13
37	2.3.4 ChimPipe	14
38	2.4 Machine Learning Approaches for Chimera and Sequence Quality	
39	Detection	15
40	2.4.1 Feature-Based Representations of Genomic Sequences . . .	16
41	2.5 Synthesis of Chimera Detection Approaches	18
42	3 Research Methodology	21
43	3.1 Research Activities	21
44	3.1.1 Data Collection	22
45	3.1.2 Bioinformatics Tools Pipeline	26
46	3.1.3 Machine Learning Model Development	29
47	3.1.4 Model Benchmarking, Hyperparameter Optimization, and	
48	Evaluation	30
49	3.1.5 Feature Importance and Interpretation	31

50	3.1.6 Validation and Testing	32
51	3.1.7 Documentation	33
52	3.2 Calendar of Activities	34

⁵³ List of Figures

⁵⁴	3.1 Process Diagram of Special Project	22
---------------	--	----

List of Tables

⁵⁵	2.1 Comparison of Chimera Detection Methods	19
⁵⁶	3.1 Timetable of Activities	34
⁵⁷		

⁵⁸ **Chapter 1**

⁵⁹ **Introduction**

⁶⁰ **1.1 Overview**

⁶¹ The rapid advancement of next-generation sequencing (NGS) technologies has
⁶² transformed genomic research by enabling high-throughput and cost-effective
⁶³ DNA analysis (Metzker, 2010). Among current platforms, Illumina sequencing
⁶⁴ remains the most widely adopted, capable of producing millions of short reads
⁶⁵ that can be assembled into reference genomes or analyzed for genetic variation
⁶⁶ (Bentley et al., 2008; Glenn, 2011). Despite its high base-calling accuracy,
⁶⁷ Illumina sequencing is prone to artifacts introduced during library preparation,
⁶⁸ particularly polymerase chain reaction (PCR)-induced chimeras, which are ar-
⁶⁹ tificial hybrid sequences that do not exist in the true genome (Judo, Wedel, &
⁷⁰ Wilson, 1998).

⁷¹ PCR chimeras form when incomplete extension products from one template

72 anneal to an unrelated DNA fragment and are extended, creating recombinant
73 reads (Qiu et al., 2001). In mitochondrial genome assembly, such artifacts are
74 especially problematic because the mitochondrial genome is small, circular, and
75 often repetitive (Boore, 1999; Cameron, 2014). Even a small number of chimeric
76 or misjoined reads can reduce assembly contiguity and introduce false junctions
77 during organelle genome reconstruction (Dierckxsens, Mardulyn, & Smits, 2017;
78 Hahn, Bachmann, & Chevreux, 2013; Jin et al., 2020). Existing assembly tools
79 such as GetOrganelle and MITObim assume that input reads are largely free of
80 such artifacts (Hahn et al., 2013; Jin et al., 2020). Consequently, undetected
81 chimeras may produce fragmented assemblies or misidentified organellar bound-
82 aries. To ensure accurate reconstruction of mitochondrial genomes, a reliable
83 method for detecting and filtering PCR-induced chimeras before assembly is es-
84 sential.

85 This study focuses on mitochondrial sequencing data from the genus *Sar-*
86 *dinella*, a group of small pelagic fishes widely distributed in Philippine waters.
87 Among them, *Sardinella lemuru* (Bali sardinella) is one of the country's most
88 abundant and economically important species, providing protein and livelihood
89 to coastal communities (Labrador, Agmata, Palermo, Ravago-Gotanco, & Pante,
90 2021; Willette, Bognot, Mutia, & Santos, 2011). Accurate mitochondrial assem-
91 blies are critical for understanding its population genetics, stock structure, and
92 evolutionary history. However, assembly pipelines often encounter errors or fail
93 to complete due to undetected chimeric reads. To address this gap, this research
94 introduces MitoChime, a machine learning pipeline designed to detect and filter
95 PCR-induced chimeric reads using both alignment-based and sequence-derived
96 statistical features. The tool aims to provide bioinformatics laboratories, partic-

97 ularly the Philippine Genome Center Visayas (PGC Visayas), with an efficient
98 solution for improving mitochondrial genome reconstruction.

99 1.2 Problem Statement

100 While NGS technologies have revolutionized genomic data acquisition, the ac-
101 curacy of mitochondrial genome assembly remains limited by artifacts produced
102 during PCR amplification. These chimeric reads can distort assembly graphs and
103 cause misassemblies, with particularly severe effects in small, circular mitochon-
104 drial genomes (Boore, 1999; Cameron, 2014). Existing assembly pipelines such
105 as GetOrganelle, MITObim, and NOVOPlasty assume that sequencing reads are
106 free of such artifacts (Dierckxsens et al., 2017; Hahn et al., 2013; Jin et al., 2020).
107 At PGC Visayas, several mitochondrial assemblies have failed or yielded incom-
108 plete contigs despite sufficient coverage, suggesting that undetected chimeric reads
109 compromise assembly reliability. Meanwhile, existing chimera detection tools such
110 as UCHIME and VSEARCH were developed primarily for amplicon-based com-
111 munity analysis and rely heavily on reference or taxonomic comparisons (Edgar,
112 Haas, Clemente, Quince, & Knight, 2011; Rognes, Flouri, Nichols, Quince, &
113 Mahé, 2016). These approaches are unsuitable for single-species organellar data,
114 where complete reference genomes are often unavailable. Therefore, there is a
115 pressing need for a reference-independent, data-driven tool capable of detecting
116 and filtering PCR-induced chimeras in mitochondrial sequencing datasets.

₁₁₇ **1.3 Research Objectives**

₁₁₈ **1.3.1 General Objective**

₁₁₉ This study aims to develop and evaluate a machine learning-based pipeline (Mi-
₁₂₀ toChime) that detects PCR-induced chimeric reads in *Sardinella lemuru* mito-
₁₂₁ chondrial sequencing data in order to improve the quality and reliability of down-
₁₂₂ stream mitochondrial genome assemblies.

₁₂₃ **1.3.2 Specific Objectives**

₁₂₄ Specifically, the study aims to:

- ₁₂₅ 1. construct simulated *Sardinella lemuru* Illumina paired-end datasets contain-
₁₂₆ ing both clean and PCR-induced chimeric reads,
- ₁₂₇ 2. extract alignment-based and sequence-based features such as k-mer compo-
₁₂₈ sition, junction complexity, and split-alignment counts from both clean and
₁₂₉ chimeric reads,
- ₁₃₀ 3. train, validate, and compare supervised machine-learning models for classi-
₁₃₁ fying reads as clean or chimeric,
- ₁₃₂ 4. determine feature importance and identify indicators of PCR-induced
₁₃₃ chimerism,
- ₁₃₄ 5. integrate the optimized classifier into a modular and interpretable pipeline
₁₃₅ deployable on standard computing environments at PGC Visayas.

136 1.4 Scope and Limitations of the Research

137 This study focuses on detecting PCR-induced chimeric reads in Illumina paired-
138 end mitochondrial sequencing data from *Sardinella lemuru*. The decision to re-
139 strict the taxonomic scope to a single species is based on four considerations:
140 (1) to limit interspecific variation in mitochondrial genome size, GC content, and
141 repetitive regions so that differences in read patterns can be attributed more di-
142 rectly to PCR-induced chimerism; (2) to align the analysis with relevant *S. lemuru*
143 sequencing projects at PGC Visayas; (3) to take advantage of the availability of *S.*
144 *lemuru* mitochondrial assemblies and raw datasets in public repositories such as
145 the National Center for Biotechnology Information (NCBI), which facilitates refer-
146 ence selection and benchmarking; and (4) to develop a tool that directly supports
147 local studies on *S. lemuru* population structure and fisheries management.

148 The study emphasizes `wgsim`-based simulations and selected empirical mito-
149 chondrial datasets from *S. lemuru*. It excludes naturally occurring chimeras, nu-
150 clear mitochondrial pseudogenes (NUMTs), and large-scale assembly rearrange-
151 ments in nuclear genomes. Feature extraction is restricted to low-dimensional
152 alignment and sequence statistics, such as k-mer frequency profiles, GC content,
153 read length, soft and hard clipping metrics, split-alignment counts, and map-
154 ping quality, rather than high-dimensional deep learning embeddings. This de-
155 sign keeps model behaviour interpretable and ensures that the pipeline can be
156 run on standard workstations at PGC Visayas. Testing on long-read platforms
157 (e.g., Nanopore, PacBio) and other taxa is outside the scope of this project; the
158 implemented pipeline is evaluated only on short-read *S. lemuru* datasets.

¹⁵⁹ 1.5 Significance of the Research

¹⁶⁰ This research provides both methodological and practical contributions to mi-
¹⁶¹tochondrial genomics and bioinformatics. First, MitoChime filters PCR-induced
¹⁶² chimeric reads prior to genome assembly, with the goal of improving the con-
¹⁶³tiguity and correctness of *Sardinella lemuru* mitochondrial assemblies. Second,
¹⁶⁴ it replaces informal manual curation with a documented workflow, improving au-
¹⁶⁵tomation and reproducibility. Third, the pipeline is designed to run on computing
¹⁶⁶ infrastructures commonly available in regional laboratories, enabling routine use
¹⁶⁷ at facilities such as PGC Visayas. Finally, more reliable mitochondrial assemblies
¹⁶⁸ for *S. lemuru* provide a stronger basis for downstream applications in the field of
¹⁶⁹ fisheries and genomics.

¹⁷⁰ **Chapter 2**

¹⁷¹ **Review of Related Literature**

¹⁷² This chapter presents an overview of the literature relevant to the study. It
¹⁷³ discusses the biological and computational foundations underlying mitochondrial
¹⁷⁴ genome analysis and assembly, as well as existing tools, algorithms, and techniques
¹⁷⁵ related to chimera detection and genome quality assessment. The chapter aims to
¹⁷⁶ highlight the strengths, limitations, and research gaps in current approaches that
¹⁷⁷ motivate the development of the present study.

¹⁷⁸ **2.1 The Mitochondrial Genome**

¹⁷⁹ Mitochondrial genome (mtDNA) is a small, typically circular molecule found in
¹⁸⁰ most eukaryotes. It encodes essential genes involved in oxidative phosphorylation
¹⁸¹ and energy metabolism. Because of its conserved structure, mtDNA has become
¹⁸² a valuable genetic marker for studies in population genetics and phylogenetics
¹⁸³ (Anderson et al., 1981; Boore, 1999). In animal species, the mitochondrial genome

ranges from 15–20 kilobase and contains 13 protein-coding genes, 22 tRNAs, and two rRNAs arranged compactly without introns (Gray, 2012). In comparison to nuclear DNA, the ratio of the number of copies of mtDNA is higher and has simple organization which make it particularly suitable for genome sequencing and assembly studies (Dierckxsens et al., 2017).

2.1.1 Mitochondrial Genome Assembly

Mitochondrial genome assembly refers to the reconstruction of the complete mitochondrial DNA (mtDNA) sequence from raw or fragmented sequencing reads. It is conducted to obtain high-quality, continuous representations of the mitochondrial genome that can be used for a wide range of analyses, including species identification, phylogenetic reconstruction, evolutionary studies, and investigations of mitochondrial diseases. Because mtDNA evolves rapidly, its assembled sequence provides valuable insights into population structure, lineage divergence, and adaptive evolution across taxa (Boore, 1999). Compared to nuclear genome assembly, assembling the mitochondrial genome is often considered more straightforward but still encounters technical challenges such as the formation of chimeric reads. Commonly used tools for mitogenome assembly such as GetOrganelle and MITObim operate under the assumption of organelle genome circularity, and are vulnerable when chimeric reads disrupt this circular structure, resulting in assembly errors (Hahn et al., 2013; Jin et al., 2020).

204 2.2 PCR Amplification and Chimera Formation

205 PCR plays an important role in NGS library preparation, as it amplifies target
206 DNA fragments for downstream analysis. However as previously mentioned, the
207 amplification process can also introduce chimeric reads which compromises the
208 quality of the input reads supplied to sequencing or assembly workflows. Chimeras
209 typically arise when incomplete extension occurs during a PCR cycle. This causes
210 the DNA polymerase to switch from one template to another and generate hy-
211 brid recombinant molecules (Judo et al., 1998). Artificial chimeras are produced
212 through such amplification errors, whereas biological chimeras occur naturally
213 through genomic rearrangements or transcriptional events.

214 In the context of amplicon-based sequencing, the presence of chimeras can in-
215 flate estimates of genetic or microbial diversity and may cause misassemblies dur-
216 ing genome reconstruction. Qin et al. (2023) has reported that chimeric sequences
217 may account for more than 10% of raw reads in amplicon datasets. This artifact
218 tends to be most prominent among rare operational taxonomic units (OTUs) or
219 singletons, which are sometimes misinterpreted as novel diversity, further caus-
220 ing the complication of microbial diversity analyses (Gonzalez, Zimmermann, &
221 Saiz-Jimenez, 2004). As such, determining and minimizing PCR-induced chimera
222 formation is vital for improving the quality of mitochondrial genome assemblies,
223 and ensuring the reliability of amplicon sequencing data.

224 **2.3 Existing Traditional Approaches for Chimera**

225 **Detection**

226 Several computational tools have been developed to identify chimeric sequences in
227 NGS datasets. These tools generally fall into two categories: reference-based and
228 de novo approaches. Reference-based chimera detection, also known as database-
229 dependent detection, is one of the earliest and most widely used computational
230 strategies for identifying chimeric sequences in amplicon-based community studies.
231 These methods rely on the comparison of each query sequence against a curated,
232 high-quality database of known, non-chimeric reference sequences (Edgar et al.,
233 2011).

234 On the other hand, the de novo chimera detection, also referred to as reference-
235 free detection, represents an alternative computational paradigm that identifies
236 chimeric sequences without reliance on external reference databases. This method
237 infer chimeras based on internal relationships among the sequences present within
238 the dataset itself, making it particularly advantageous in studies of under explored
239 or taxonomically diverse communities where comprehensive reference databases
240 are unavailable or incomplete (Edgar, 2016; Edgar et al., 2011). The underlying
241 assumption on this method is that during PCR, true biological sequences are
242 generally more abundant as they are amplified early and dominate the read pool,
243 whereas chimeric sequences appear later and are generally less abundant. The
244 de novo approach leverage this abundance hierarchy, treating the most abundant
245 sequences as supposed parents and testing whether less abundant sequences can
246 be reconstructed as mosaics of these templates. Compositional and structural
247 similarity are also evaluated to check whether different regions of a candidate

248 sequence correspond to distinct high-abundance sequences.

249 In practice, many modern bioinformatics pipelines combine both paradigms
250 sequentially: an initial de novo step identifies dataset-specific chimeras, followed
251 by a reference-based pass that removes remaining artifacts relative to established
252 databases (Edgar, 2016). These two methods of detection form the foundation of
253 tools such as UCHIME and later UCHIME2.

254 2.3.1 UCHIME

255 UCHIME is one of the most widely used computational tools for detecting chimeric
256 sequences in amplicon sequencing data, as it serves as a critical quality control
257 step to prevent the misinterpretation of PCR artifacts as novel biological diversity.
258 The algorithm operates by searching for a model (M) where a query (Q) sequence
259 can be perfectly explained as a combination of two parent sequences, denoted as
260 A and B (Edgar et al., 2011).

261 In reference mode, UCHIME divides the query into four chunks and maps
262 them to a trusted chimeric-free database to identify candidate parents. It then
263 constructs a three-way alignment to calculate a score based on “votes.” A “Yes”
264 vote indicates the query aligns with parent A in one region and parent B in an-
265 other, while a “No” vote penalizes the score if the query diverges from the expected
266 chimeric model. In de novo mode, the algorithm operationalizes the abundance
267 skew principle described in Section 2.3. Instead of using an external database,
268 UCHIME dynamically treats the sample’s own high-abundance sequences as a
269 reference database, testing if lower-abundance sequences can be reconstructed as

270 mosaics of these internal ancestors (Edgar et al., 2011).

271 Despite its high sensitivity, UCHIME has inherent limitations rooted in
272 sequence divergence and database quality. The algorithm struggles to detect
273 chimeras formed from parents that are very closely related, specifically when the
274 sequence divergence between parents is less than roughly 0.8%, as the signal-to-
275 noise ratio becomes too low to distinguish a crossover event from sequencing error
276 (Edgar et al., 2011). Furthermore, in reference mode, the accuracy is strictly
277 bound by the completeness of the database; if true parents are absent, the tool
278 may fail to identify the chimera or produce false positives. Similarly, the de novo
279 mode relies on the assumption that parents are present and sufficiently more
280 abundant in the sample, which may not hold true in unevenly amplified samples
281 or complex communities.

282 **2.3.2 UCHIME2**

283 Building upon the original algorithm, UCHIME2 was developed to address the
284 nuances of high-resolution amplicon sequencing. A key contribution of the
285 UCHIME2 study was the critical re-evaluation of chimera detection benchmarks.
286 In the UCHIME2 paper (Edgar, 2016) and the UCHIME in practice website
287 (Edgar, n.d), the author has noted that the accuracy results reported in the
288 original UCHIME paper were “highly over-optimistic” because they relied on
289 unrealistic benchmark designs where parent sequences were assumed to be 100%
290 known and present. UCHIME2 introduced more rigorous testing (the CHSIMA
291 benchmark), revealing that “fake models,” where a valid biological sequence
292 perfectly mimics a chimera of two other valid sequences, are far more common

than previously assumed. This discovery suggests that error-free detection is impossible in principle (Edgar, 2016). Another notable improvement is the introduction of multiple application-specific modes that allow users to tailor the algorithm’s performance to the characteristics of their datasets. The following parameter presets: denoised, balanced, sensitive, specific, and high-confidence, enable researchers to optimize the balance between sensitivity and specificity according to the goals of their analysis.

However despite these advancements, the practical application of UCHIME2 requires caution. The author explicitly advises against using UCHIME2 as a stand-alone tool in standard OTU clustering or denoising pipelines. Using UCHIME2 as an independent filtering step in these workflows is discouraged, as it often results in significantly higher error rates, increasing both false positives (discarding valid sequences) and false negatives (retaining chimeras) (Edgar, 2016).

2.3.3 CATch

As previously mentioned, UCHIME (Edgar et al., 2011) relied on alignment-based sequences in amplicon data. However, researchers soon observed that different algorithms often produced inconsistent predictions. A sequence might be identified as chimeric by one tool but classified as non-chimeric by another, resulting in unreliable filtering outcomes across studies.

To address these inconsistencies, Mysara, Saeys, Leys, Raes, and Monsieurs (2015) developed the Classifier for Amplicon Tool Chimeras (CATCh), which rep-

315 resents the first ensemble machine learning system designed for chimera detection
316 in 16S rRNA amplicon sequencing. Rather than depending on a single detec-
317 tion strategy, CATCh integrates the outputs of several established tools, includ-
318 ing UCHIME, ChimeraSlayer, DECIPHER, Pintail, and Perseus. The individual
319 scores and binary decisions generated by these tools are used as input features for
320 a supervised learning model. The algorithm employs a Support Vector Machine
321 (SVM) with a Pearson VII Universal Kernel (PUK) to determine optimal weight-
322 ings among the input features and to assign each sequence a probability of being
323 chimeric.

324 Benchmarking in both reference-based and de novo modes demonstrated signif-
325 icant performance improvements. CATCh achieved sensitivities of approximately
326 85 percent in reference-based mode and 92 percent in de novo mode, with corre-
327 sponding specificities of approximately 96 percent and 95 percent. These results
328 indicate that CATCh detected 7 to 12 percent more chimeras than any individual
329 algorithm while maintaining high precision.

330 2.3.4 ChimPipe

331 Among the available tools for chimera detection, ChimPipe is a pipeline developed
332 to identify chimeric sequences such as biological chimeras. It uses both discordant
333 paired-end reads and split-read alignments to improve the accuracy and sensitivity
334 of detecting biological chimeras (Rodriguez-Martin et al., 2017). By combining
335 these two sources of information, ChimPipe achieves better precision than meth-
336 ods that depend on a single type of indicator.

337 The pipeline works with many eukaryotic species that have available genome
338 and annotation data (Rodriguez-Martin et al., 2017). It can also predict multiple
339 isoforms for each gene pair and identify breakpoint coordinates that are useful
340 for reconstructing and verifying chimeric transcripts. Tests using both simulated
341 and real datasets have shown that ChimPipe maintains high accuracy and reliable
342 performance.

343 ChimPipe lets users adjust parameters to fit different sequencing protocols or
344 organism characteristics. Experimental results have confirmed that many chimeric
345 transcripts detected by the tool correspond to functional fusion proteins, demon-
346 strating its utility for understanding chimera biology and its potential applications
347 in disease research (Rodriguez-Martin et al., 2017).

348 **2.4 Machine Learning Approaches for Chimera 349 and Sequence Quality Detection**

350 Traditional chimera detection tools rely primarily on heuristic or alignment-based
351 rules. Recent advances in machine learning (ML) have demonstrated that models
352 trained on sequence-derived features can effectively capture compositional and
353 structural patterns in biological sequences. Although most existing ML systems
354 such as those used for antibiotic resistance prediction, taxonomic classification,
355 or viral identification are not specifically designed for chimera detection, they
356 highlight how data-driven models can outperform similarity-based heuristics by
357 learning intrinsic sequence signatures. In principle, ML frameworks can integrate
358 indicators such as k-mer frequencies, GC-content variation and split-alignment

359 metrics to identify subtle anomalies that may indicate a chimeric origin (Arango
360 et al., 2018; Liang, Bible, Liu, Zou, & Wei, 2020; Ren et al., 2020).

361 **2.4.1 Feature-Based Representations of Genomic Se-**
362 **quences**

363 In genomic analysis, feature extraction converts DNA sequences into numerical
364 representations suitable for ML algorithms. A common approach is k-mer fre-
365 quency analysis, where normalized k-mer counts form the feature vector (Vervier,
366 Mahé, Tournoud, Veyrieras, & Vert, 2015). These features effectively capture lo-
367 cal compositional patterns that often differ between authentic and chimeric reads.

368 In particular, deviations in k-mer profiles between adjacent read segments can
369 serve as a compositional signature of template-switching events. Additional de-
370 scriptors such as GC content and sequence entropy can further distinguish se-
371 quence types; in metagenomic classification and virus detection, k-mer-based fea-
372 tures have shown strong performance and robustness to noise (Ren et al., 2020;
373 Vervier et al., 2015). For chimera detection specifically, abrupt shifts in GC or k-
374 mer composition along a read can indicate junctions between parental fragments.
375 Windowed feature extraction enables models to capture these discontinuities that
376 rule-based algorithms may overlook.

377 Machine learning models can also leverage alignment-derived features such as
378 the frequency of split alignments, variation in mapping quality, and local cover-
379 age irregularities. Split reads and discordant read pairs are classical indicators
380 of genomic junctions and have been formalized in probabilistic frameworks for
381 structural-variant discovery that integrate multiple evidence types (Layer, Hall, &

Quinlan, 2014). Similarly, long-read tools such as Sniffles employ split-alignment and coverage anomalies to accurately localize breakpoints (Sedlazeck et al., 2018). Modern aligners such as Minimap2 (Li, 2018) output supplementary (SA tags) and secondary alignments as well as chaining and alignment-score statistics that can be summarized into quantitative predictors for machine-learning models. These alignment-signal features are particularly relevant to PCR-induced mitochondrial chimeras, where template-switching events produce reads partially matching distinct regions of the same or related genomes. Integrating such cues within a supervised-learning framework enables artifact detection even in datasets lacking complete or perfectly assembled references.

A further biologically grounded descriptor is the length of microhomology at putative junctions. Microhomology refers to short, shared sequences, often in the range of a few to tens of base pairs that are near breakpoints where template-switching events typically happen. Studies of double strand break repair and structural variation have demonstrated that the length of microhomology correlates with the likelihood of microhomology-mediated end joining (MMEJ) or fork-stalled template-switching pathways (Sfeir & Symington, 2015). In the context of PCR-induced chimeras, template switching during amplification often leaves short identical sequences at the junction of two concatenated fragments. Quantifying the longest exact suffix–prefix overlap at each candidate breakpoint thus provides a mechanistic signature of chimerism and complements both compositional (k-mer) and alignment (SA count) features.

404 2.5 Synthesis of Chimera Detection Approaches

405 To provide an integrated overview of the literature discussed in this chapter, Ta-
406 ble 2.1 summarizes the major chimera detection studies, their methodological
407 approaches, and their known limitations.

Table 2.1: Comparison of Chimera Detection Methods

Methods	Approach	Limitations
Reference-based Chimera Detection	Compares query sequences against curated, non-chimeric reference databases; identifies mosaic sequences by evaluating similarity to known templates.	Depends heavily on completeness and quality of reference databases; often fails when novel taxa or missing parent sequences are present; reduced accuracy for low-divergence chimeras.
De novo Chimera Detection	Identifies chimeras using only internal dataset relationships; relies on abundance patterns and compositional similarity; reconstructs sequences as mosaics of high-abundance parents.	Assumes true sequences are more abundant—fails when amplification bias distorts abundance; struggles with evenly abundant parental sequences; can misclassify highly similar true variants.
UCHIME	Alignment-based chimera detection; segments query sequence, identifies parent candidates, performs 3-way alignment, and computes chimera scores; supports both reference-based and de novo modes.	Accuracy inflated in original benchmarks; suffers under incomplete databases; poor performance on low-divergence chimeras; sensitive to sequencing errors; misclassifies when parents are missing.
UCHIME2	Improved initial UCHIME benchmarking; offers multiple sensitivity/specificity modes; more robust with incomplete references; higher sensitivity.	Cannot achieve perfect accuracy due to “perfect fake models”; genuine variants may be indistinguishable from artificial recombinants; theoretical detection limit remains.
CATCh	First ML ensemble tool for 16S chimera detection; integrates outputs of UCHIME, ChimeraSlayer, DECIPHER, Pintail, Perseus via SVM classifier; significantly improves sensitivity and specificity.	Depends on performance of underlying tools; ML model limited to features they output; ensemble can still misclassify in datasets with extreme novelty or low coverage.
ChimPipe	Pipeline for detecting fusion genes and transcript-derived chimeras in RNA-seq; uses discordant paired-end reads and split-alignments; predicts isoforms and breakpoint coordinates.	Designed for RNA-seq, not amplicons; needs high-quality genome and annotation; computationally heavier; limited to organisms with reference genomes.

408 Across existing studies, no single approach reliably detects all forms of chimeric
409 sequences, particularly those generated by PCR-induced template switching in
410 mitochondrial genomes. Reference-based tools perform poorly when parental se-
411 quences are absent; de novo methods rely strongly on abundance assumptions;
412 alignment-based systems show reduced sensitivity to low-divergence chimeras; and
413 ensemble methods inherit the limitations of their component algorithms. RNA-
414 seq-oriented pipelines likewise do not generalize well to organelle data. Although
415 machine learning approaches offer promising feature-based detection, they are
416 rarely applied to mitochondrial genomes and are not trained specifically on PCR-
417 induced organelle chimeras. These limitations indicate a clear research gap: the
418 need for a specialized, feature-driven classifier tailored to mitochondrial PCR-
419 induced chimeras that integrates k-mer composition, split-alignment signals, and
420 micro-homology features to achieve more accurate detection than current heuristic
421 or alignment-based tools.

⁴²² Chapter 3

⁴²³ Research Methodology

⁴²⁴ This chapter outlines the steps involved in completing the study, including data
⁴²⁵ gathering, generating simulated mitochondrial Illumina reads, preprocessing and
⁴²⁶ indexing the data, developing a bioinformatics pipeline to extract key features,
⁴²⁷ applying machine learning algorithms for chimera detection, and validating and
⁴²⁸ comparing model performance.

⁴²⁹ 3.1 Research Activities

⁴³⁰ As illustrated in Figure 3.1, this study carried out a sequence of procedures to
⁴³¹ detect PCR-induced chimeric reads in mitochondrial genomes. The process began
⁴³² with collecting a mitochondrial reference sequence of *Sardinella lemuru* from the
⁴³³ National Center for Biotechnology Information (NCBI) database, which was used
⁴³⁴ as a reference for generating simulated clean and chimeric reads. These reads
⁴³⁵ were subsequently indexed and mapped. The resulting collections then passed

436 through a bioinformatics pipeline that extracted k-mer profiles, supplementary
437 alignment (SA) features, and microhomology information to prepare the data for
438 model construction. The machine learning model was trained using the processed
439 input, and its precision and accuracy were assessed. It underwent tuning until it
440 reached the desired performance threshold, after which it proceeded to validation
441 and will undergo testing.

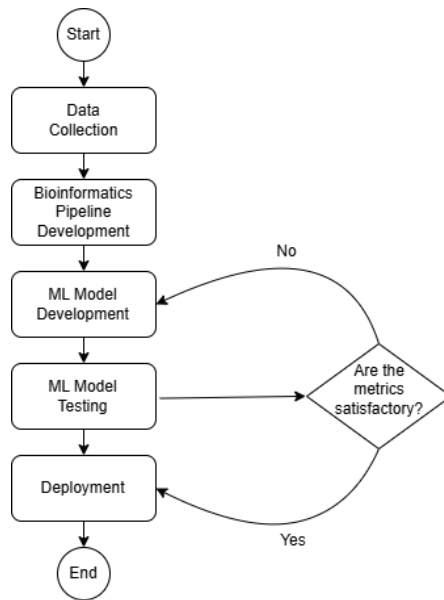


Figure 3.1: Process Diagram of Special Project

442 3.1.1 Data Collection

443 The mitochondrial genome reference sequence of *S. lemuru* was obtained from the
444 NCBI database (accession number NC_039553.1) in FASTA format. This sequence
445 served as the basis for generating simulated reads for model development.

446 This step was scheduled to begin in the first week of November 2025 and
447 expected to be completed by the end of that week, with a total duration of ap-

448 proximately one (1) week.

449 **Data Preprocessing**

450 To reduce manual repetition, all steps in the simulation and preprocessing pipeline
451 were executed using a custom script in Python (Version 3.11). The script runs
452 each stage, including read simulation, reference indexing, mapping, and alignment
453 processing, in a fixed sequence.

454 Sequencing data were simulated from the NCBI reference genome using `wgsim`
455 (Version 1.13). First, a total of 10,000 paired-end fragments were simulated,
456 producing 20,000 reads (10,000 forward and 10,000 reverse) from the the original
457 reference (`original_reference.fasta`) and and designated as clean reads using
458 the command:

```
459 wgsim -1 150 -2 150 -r 0 -R 0 -X 0 -e 0.001 -N 10000 \  
460           original_reference.fasta ref1.fastq ref2.fastq
```

461 The command parameters are as follows:

- 462 • `-1` and `-2`: read lengths of 150 base pairs for each paired-end read.
- 463 • `-r`, `-R`, `-X`: mutation rate, fraction of indels, and indel extension probability,
464 all set to a default value of 0.
- 465 • `-e`: base error rate, set to 0.001 to simulate realistic sequencing errors.
- 466 • `-N`: number of read pairs, set to 10,000.

467 Chimeric sequences were then generated from the same NCBI reference using a
468 separate Python script. Two non-adjacent segments were randomly selected such
469 that their midpoint distances fell within specified minimum and maximum thresh-
470 olds. The script attempts to retain microhomology, or short identical sequences
471 at segment junctions, to mimic PCR-induced template switching. The resulting
472 chimeras were written to `chimera_reference.fasta`, with headers recording seg-
473 ment positions and microhomology length. The `chimera_reference.fasta` was
474 processed with `wgsim` to simulate 10,000 paired-end fragments, generating 20,000
475 chimeric reads (10,000 forward reads in `chimeric1.fastq` and 10,000 reverse reads
476 in `chimeric2.fastq`) using the command format.

477 Next, a `minimap2` index of the reference genome was created using:

```
478 minimap2 -d ref.mmi original_reference.fasta
```

479 Minimap2 (Version 2.28) is a tool used to map reads to a reference genome.
480 The index `ref.mmi` of the original reference sequence is required by `minimap2` for
481 efficient read mapping. Mapping allows extraction of alignment features from each
482 read, which were used as input for the machine learning model. The simulated
483 clean and chimeric reads were then mapped to the reference index as follows:

```
484 minimap2 -ax sr -t 8 ref.mmi ref1.fastq ref2.fastq > clean.sam
```

```
485 minimap2 -ax sr -t 8 ref.mmi \  
486 chimeric1.fastq chimeric2.fastq > chimeric.sam
```

487 Here, `-ax sr` specifies short-read alignment mode, and `-t 8` uses 8 CPU

488 threads. The resulting clean and chimeric SAM files contain the alignment posi-
489 tions of each read relative to the original reference genome.

490 The SAM files were then converted to BAM format, sorted, and indexed using

491 `samtools` (Version 1.20):

```
492 samtools view -bS clean.sam -o clean.bam  
493 samtools view -bS chimeric.sam -o chimeric.bam  
494  
495 samtools sort clean.bam -o clean.sorted.bam  
496 samtools index clean.sorted.bam  
497  
498 samtools sort chimeric.bam -o chimeric.sorted.bam  
499 samtools index chimeric.sorted.bam
```

500 BAM files are the compressed binary version of SAM files, which enables faster
501 processing and reduced storage. Sorting arranges reads by genomic coordinates,
502 and indexing allows detection of SA as a feature for the machine learning model.

503 The total number of simulated reads was expected to be 40,000. The final col-
504 lection of reads contained 19,984 clean reads and 20,000 chimeric reads (39,984 en-
505 tries in total), providing a roughly balanced distribution between the two classes.
506 After alignment with `minimap2`, only 19,984 clean reads remained because un-
507 mapped reads were not included in the BAM file. Some sequences failed to align
508 due to the 5% error rate defined during `wgsim` simulation, which produced mis-
509 matches that caused certain reads to fall below the aligner's matching threshold.

510 This whole process is scheduled to start in the second week of November 2025

511 and is expected to be completed by the last week of November 2025, with a total
512 duration of approximately three (3) weeks.

513 **3.1.2 Bioinformatics Tools Pipeline**

514 A bioinformatics pipeline will be developed and implemented to extract the neces-
515 sary analytical features. This pipeline will function as a reproducible and modular
516 workflow that accepts FASTQ and BAM/SAM file inputs, processes them using
517 tools such as `samtools` and `jellyfish` (Version 2.3.1), and produces tabular fea-
518 ture matrices (TSV) for downstream machine learning. To ensure correctness
519 and adherence to best practices, bioinformatics experts at the PGC Visayas will
520 be consulted to validate the pipeline design, feature extraction logic, and overall
521 data integrity. This stage of the study is scheduled to begin in the first week of
522 January 2026 and conclude by the last week of February 2026, with an estimated
523 total duration of approximately two (2) months.

524 The bioinformatics pipeline focuses on three principal features from the simu-
525 lated and aligned sequencing data: (1) supplementary alignment flag (SA count),
526 (2) k-mer composition difference between read segments, and (3) microhomology
527 length at potential junctions. Each of these features captures a distinct biological
528 or computational signature associated with PCR-induced chimeras.

529 **Supplementary Alignment Flag**

530 Supplementary alignment information will be assessed using the mapped and
531 sorted BAM files (`clean.sorted.bam` and `chimeric.sorted.bam`) generated

532 from the data preprocessing stage. Alignment summaries will be checked using
533 `samtools flagstat` to obtain preliminary quality-control statistics, including
534 counts of primary, secondary, and supplementary (SA) alignments.

535 Both BAM files will be converted to SAM format for detailed inspection of
536 reads in each file:

```
537 samtools view -h clean.sorted.bam -o clean.sorted.sam  
538 samtools view -h chimeric.sorted.bam -o chimeric.sorted.sam
```

539 The SAM output will be checked for reads containing the SA:Z flag, as it
540 denotes supplementary alignments. Reads exhibiting these or substantial soft-
541 clipped regions will be considered strong candidates for chimeric artifacts. A
542 custom Python script would be created to extract the alignment-derived features
543 and relevant metadata including mapping quality, SAM flag information, CIGAR-
544 based clipping, and alignment coordinates. These extracted attributes would then
545 be organized and compiled into a TSV (`.tsv`) file.

546 K-mer Composition Difference

547 Chimeric reads often comprise fragments from distinct genomic regions, resulting
548 in a compositional discontinuity between segments. Comparing k-mer frequency
549 profiles between the left and right halves of a read allows detection of such abrupt
550 compositional shifts, independent of alignment information. This will be obtained
551 using Jellyfish, a fast k-mer counting software. For each read, the sequence will
552 be divided into two segments, either at the midpoint or at empirically determined
553 breakpoints inferred from supplementary alignment data, to generate left and right

554 sequence segments. Jellyfish will then compute k-mer frequency profiles (with $k =$
555 5 or 6) for each segment. The resulting k-mer frequency vectors will be normalized
556 and compared using distance metrics such as cosine similarity or Jensen–Shannon
557 divergence to quantify compositional disparity between the two halves of the same
558 read. The resulting difference scores will be stored in a structured TSV file.

559 Microhomology Length

560 The microhomology length was computed as part of the bioinformatics pipeline.
561 For each aligned read in the BAM files, the script first inferred a breakpoint
562 using the function `infer_breakpoint`, which represents a junction between two
563 segments. Breakpoints were determined primarily from soft-clipping patterns.
564 If no soft clips were present, SA tags were used to identify potential alignment
565 discontinuities.

566 Once a breakpoint was established, the script scanned a ± 40 base pair window
567 surrounding the breakpoint and used the function `longest_suffix_prefix_overlap`
568 to identify the longest exact suffix-prefix overlap between the left and right read
569 segments. This overlap, which represents consecutive bases shared at the junc-
570 tion, was recorded as the microhomology length. Additionally, the GC content
571 of the overlapping sequence was calculated using the function `gc_content`, which
572 counts guanine (G) and cytosine (C) bases within the detected microhomology
573 and divides by the total length, yielding a proportion between 0 and 1.

574 Short microhomologies, typically 3-20 base pairs in length, are recognized sig-
575 natures of PCR-induced template switching and can promote template recombi-
576 nation (Peccoud et al., 2018). Each read was annotated after capturing both the

577 length and GC content of microhomology.

578 3.1.3 Machine Learning Model Development

579 After feature extraction, the per-read feature matrices for clean and chimeric
580 reads were merged into a single dataset. Each row corresponded to one paired-
581 end read, and columns encoded alignment-structure features (e.g., supplementary
582 alignment count and spacing between segments), CIGAR-derived soft-clipping
583 statistics (e.g., left and right soft-clipped length, total clipped bases), k-mer com-
584 position discontinuity between read segments, and microhomology descriptors
585 near candidate junctions. The resulting feature set was restricted to quantities
586 that can be computed from standard BAM/FASTQ files in typical mitochondrial
587 sequencing workflows.

588 The labelled dataset was randomly partitioned into training (80%) and test
589 (20%) subsets using stratified sampling to preserve the 1:1 ratio of clean to
590 chimeric reads. Model development and evaluation were implemented in Python
591 (Version 3.11) using the `scikit-learn`, `xgboost`, `lightgbm`, and `catboost` li-
592 braries. A broad panel of classification algorithms was then benchmarked on the
593 training data to obtain a fair comparison of different model families under identical
594 feature conditions. The panel included: a trivial dummy classifier, L2-regularized
595 logistic regression, a calibrated linear support vector machine (SVM), k -nearest
596 neighbours, Gaussian Naïve Bayes, decision-tree ensembles (Random Forest, Ex-
597 tremely Randomized Trees, and Bagging with decision trees), gradient boosting
598 methods (Gradient Boosting, XGBoost, LightGBM, and CatBoost), and a shallow
599 multilayer perceptron (MLP).

600 For each model, five-fold stratified cross-validation was performed on the train-
601 ing set. In every fold, four-fifths of the data were used for fitting and the remaining
602 one-fifth for validation. Mean cross-validation accuracy, precision, recall, F1-score
603 for the chimeric class, and area under the receiver operating characteristic curve
604 (ROC–AUC) were computed to summarize performance and rank candidate meth-
605 ods. This baseline screen allowed comparison of linear, probabilistic, neural, and
606 ensemble-based approaches and identified tree-based ensemble and boosting mod-
607 els as consistently strong performers relative to simpler baselines.

608 **3.1.4 Model Benchmarking, Hyperparameter Optimiza-
609 tion, and Evaluation**

610 Model selection and refinement proceeded in two stages. First, the cross-validation
611 results from the broad panel were used to identify a subset of competitive mod-
612 els for more detailed optimization. Specifically, ten model families were carried
613 forward: L2-regularized logistic regression, calibrated linear SVM, Random For-
614 est, ExtraTrees, Gradient Boosting, XGBoost, LightGBM, CatBoost, Bagging
615 with decision trees, and a shallow MLP. This subset spans both linear and non-
616 linear decision boundaries, but emphasizes ensemble and boosting methods, which
617 showed superior F1 and ROC–AUC in the initial benchmark.

618 Second, hyperparameter optimization was conducted for each of the ten se-
619 lected models using randomized search with five-fold stratified cross-validation
620 (`RandomizedSearchCV`). For tree-based ensembles, the search space included the
621 number of trees, maximum depth, minimum samples per split and leaf, and the
622 fraction of features considered at each split. For boosting methods, key hyper-

623 parameters such as the number of boosting iterations, learning rate, tree depth,
624 subsampling rate, and column subsampling rate were tuned. For the MLP, the
625 number and size of hidden layers, learning rate, and L_2 regularization strength
626 were varied. In all cases, the primary optimisation criterion was the F1-score of
627 the chimeric class, averaged across folds.

628 For each model family, the hyperparameter configuration with the highest
629 mean cross-validation F1-score was selected as the best-tuned estimator. These
630 tuned models were then refitted on the full training set and evaluated once on the
631 held-out test set to obtain unbiased estimates of performance. Test-set metrics in-
632 cluded accuracy, precision, recall, F1-score for the chimeric class, and ROC–AUC.
633 Confusion matrices and ROC curves were generated for the top-performing mod-
634 els to characterise common error modes, such as false negatives (missed chimeric
635 reads) and false positives (clean reads incorrectly labelled as chimeric). The final
636 model or small set of models for downstream interpretation was chosen based on
637 a combination of test-set F1-score, ROC–AUC, and practical considerations such
638 as model complexity and ease of deployment within a bioinformatics pipeline.

639 **3.1.5 Feature Importance and Interpretation**

640 To relate model decisions to biologically meaningful signals, feature-importance
641 analyses were performed on the best-performing tree-based models. Two comple-
642 mentary approaches were used. First, built-in importance measures from ensemble
643 methods (e.g., split-based importances in Random Forest and Gradient Boosting)
644 were examined to obtain an initial ranking of features based on their contribution
645 to reducing impurity. Second, model-agnostic permutation importance was com-

646 puted on the test set by repeatedly permuting each feature column while keeping
647 all others fixed and measuring the resulting decrease in F1-score. Features whose
648 permutation led to a larger performance drop were interpreted as more influential
649 for chimera detection.

650 For interpretability, individual features were grouped into four conceptual
651 families: (i) supplementary alignment and alignment-structure features (e.g., SA
652 count, spacing between alignment segments, strand consistency), (ii) CIGAR-
653 derived soft-clipping features (e.g., left and right soft-clipped length, total clipped
654 bases), (iii) k-mer composition discontinuity features (e.g., cosine distance and
655 Jensen–Shannon divergence between k-mer profiles of read segments), and (iv) mi-
656 crohomology descriptors (e.g., microhomology length and local GC content around
657 putative breakpoints). Aggregating permutation importance scores within each
658 family allowed assessment of which biological signatures contributed most strongly
659 to the classifier’s performance. This analysis provided a basis for interpreting the
660 trained models in terms of known mechanisms of PCR-induced template switching
661 and for identifying which alignment- and sequence-derived cues are most informa-
662 tive for distinguishing chimeric from clean mitochondrial reads.

663 3.1.6 Validation and Testing

664 Validation will involve both internal and external evaluations. Internal valida-
665 tion was achieved through five-fold cross-validation on the training data to verify
666 model generalization and reduce variance due to random sampling. External vali-
667 dation will be achieved through testing on the 20% hold-out dataset derived from
668 the simulated reads, which will be an unbiased benchmark to evaluate how well

669 the trained models generalized to unseen data. All feature extraction and pre-
670 processing steps were performed using the same bioinformatics pipeline to ensure
671 consistency and comparability across validation stages.

672 Comparative evaluation was performed across all candidate algorithms, in-
673 cluding a trivial dummy classifier, L2-regularized logistic regression, a calibrated
674 linear SVM, k-nearest neighbours, Gaussian Naïve Bayes, decision-tree ensembles,
675 gradient boosting methods, and a shallow MLP. This evaluation determined which
676 models demonstrated the highest predictive performance and computational effi-
677 ciency under identical data conditions. Their metrics were compared to identify
678 which algorithms were most suitable for further refinement.

679 **3.1.7 Documentation**

680 Comprehensive documentation was maintained throughout the study to ensure
681 transparency and reproducibility. All stages of the research, including data gath-
682 ering, preprocessing, feature extraction, model training, and validation, were sys-
683 tematically recorded in a `.README` file in the GitHub repository. For each ana-
684 lytical step, the corresponding parameters, software versions, and command line
685 scripts were documented to enable exact replication of results.

686 The repository structure followed standard research data management prac-
687 tices, with clear directories for datasets and scripts. Computational environments
688 were standardized using Conda, with an environment file (`environment.arm.yml`)
689 specifying dependencies and package versions to maintain consistency across sys-
690 tems.

691 For manuscript preparation and supplementary materials, Overleaf (L^AT_EX)
692 was used to produce publication-quality formatting and consistent referencing. f

693 3.2 Calendar of Activities

694 Table 3.1 presents the project timeline in the form of a Gantt chart, where each
695 bullet point corresponds to approximately one week of planned activity.

Table 3.1: Timetable of Activities

Activities (2025)	Nov	Dec	Jan	Feb	Mar	Apr	May
Data Collection and Simulation	• • •						
Bioinformatics Tools Pipeline			• • •	• • •			
Machine Learning Development			• •	• • •	• • •	• •	
Testing and Validation						• •	• • •
Documentation	• • •	• • •	• • •	• • •	• • •	• • •	• • •

⁶⁹⁶ References

- ⁶⁹⁷ Anderson, S., Bankier, A., Barrell, B., Bruijn, M., Coulson, A., Drouin, J., ...
⁶⁹⁸ Young, I. (1981, 04). Sequence and organization of the human mitochondrial
⁶⁹⁹ genome. *Nature*, *290*, 457-465. doi: 10.1038/290457a0
- ⁷⁰⁰ Arango, G., Garner, E., Pruden, A., Heath, L., Vikesland, P., & Zhang, L. (2018,
⁷⁰¹ 02). Deeparg: A deep learning approach for predicting antibiotic resistance
⁷⁰² genes from metagenomic data. *Microbiome*, *6*. doi: 10.1186/s40168-018
⁷⁰³ -0401-z
- ⁷⁰⁴ Bentley, D. R., Balasubramanian, S., Swerdlow, H. P., Smith, G. P., Milton, J.,
⁷⁰⁵ Brown, C. G., ... Smith, A. J. (2008). Accurate whole human genome
⁷⁰⁶ sequencing using reversible terminator chemistry. *Nature*, *456*(7218), 53–
⁷⁰⁷ 59. doi: 10.1038/nature07517
- ⁷⁰⁸ Boore, J. L. (1999). Animal mitochondrial genomes. *Nucleic Acids Research*,
⁷⁰⁹ *27*(8), 1767–1780. doi: 10.1093/nar/27.8.1767
- ⁷¹⁰ Cameron, S. L. (2014). Insect mitochondrial genomics: Implications for evolution
⁷¹¹ and phylogeny. *Annual Review of Entomology*, *59*, 95–117. doi: 10.1146/
⁷¹² annurev-ento-011613-162007
- ⁷¹³ Dierckxsens, N., Mardulyn, P., & Smits, G. (2017). Novoplasty: de novo assembly
⁷¹⁴ of organelle genomes from whole genome data. *Nucleic Acids Research*,

- 715 45(4), e18. doi: 10.1093/nar/gkw955
- 716 Edgar, R. C. (2016). Uchime2: improved chimera prediction for amplicon se-
717 quencing. *bioRxiv*. Retrieved from <https://api.semanticscholar.org/>
718 CorpusID:88955007
- 719 Edgar, R. C. (n.d.). *Uchime in practice*. Retrieved from https://www.drive5.com/usearch/manual7/uchime_practical.html
- 720 Edgar, R. C., Haas, B. J., Clemente, J. C., Quince, C., & Knight, R. (2011).
721 Uchime improves sensitivity and speed of chimera detection. *Bioinformatics*,
722 27(16), 2194–2200. doi: 10.1093/bioinformatics/btr381
- 723 Glenn, T. C. (2011). Field guide to next-generation dna sequencers. *Molecular
724 Ecology Resources*, 11(5), 759–769. doi: 10.1111/j.1755-0998.2011.03024.x
- 725 Gonzalez, J. M., Zimmermann, J., & Saiz-Jimenez, C. (2004, 09). Evalu-
726 ating putative chimeric sequences from pcr-amplified products. *Bioin-
727 formatics*, 21(3), 333-337. Retrieved from <https://doi.org/10.1093/bioinformatics/bti008>
728 doi: 10.1093/bioinformatics/bti008
- 729 Gray, M. W. (2012). Mitochondrial evolution. *Cold Spring Harbor perspectives
730 in biology*, 4. Retrieved from <https://doi.org/10.1101/cshperspect.a011403>
731 doi: 10.1101/cshperspect.a011403
- 732 Hahn, C., Bachmann, L., & Chevreux, B. (2013). Reconstructing mitochondrial
733 genomes directly from genomic next-generation sequencing reads—a baiting
734 and iterative mapping approach. *Nucleic Acids Research*, 41(13), e129. doi:
735 10.1093/nar/gkt371
- 736 Jin, J.-J., Yu, W.-B., Yang, J., Song, Y., dePamphilis, C. W., Yi, T.-S., & Li,
737 D.-Z. (2020). Getorganelle: a fast and versatile toolkit for accurate de
738 novo assembly of organelle genomes. *Genome Biology*, 21(1), 241. doi:
739 10.1186/s13059-020-02154-5
- 740

- 741 Judo, M. S. B., Wedel, W. R., & Wilson, B. H. (1998). Stimulation and sup-
742 pression of pcr-mediated recombination. *Nucleic Acids Research*, *26*(7),
743 1819–1825. doi: 10.1093/nar/26.7.1819
- 744 Labrador, K., Agmata, A., Palermo, J. D., Ravago-Gotanco, R., & Pante, M. J.
745 (2021). Mitochondrial dna reveals genetically structured haplogroups of
746 bali sardinella (sardinella lemuru) in philippine waters. *Regional Studies in*
747 *Marine Science*, *41*, 101588. doi: 10.1016/j.rsma.2020.101588
- 748 Layer, R., Hall, I., & Quinlan, A. (2014, 10). Lumpy: A probabilistic framework
749 for structural variant discovery. *Genome Biology*, *15*. doi: 10.1186/gb-2014
750 -15-6-r84
- 751 Li, H. (2018, 05). Minimap2: pairwise alignment for nucleotide sequences. *Bioin-*
752 *formatics*, *34*(18), 3094-3100. Retrieved from <https://doi.org/10.1093/bioinformatics/bty191> doi: 10.1093/bioinformatics/bty191
- 753 Liang, Q., Bible, P. W., Liu, Y., Zou, B., & Wei, L. (2020, 02). Deepmi-
754 crobes: taxonomic classification for metagenomics with deep learning. *NAR*
755 *Genomics and Bioinformatics*, *2*(1), lqaa009. Retrieved from <https://doi.org/10.1093/nargab/lqaa009> doi: 10.1093/nargab/lqaa009
- 756 Metzker, M. L. (2010). Sequencing technologies — the next generation. *Nature*
757 *Reviews Genetics*, *11*(1), 31–46. doi: 10.1038/nrg2626
- 758 Mysara, M., Saeys, Y., Leys, N., Raes, J., & Monsieurs, P. (2015). Catch,
759 an ensemble classifier for chimera detection in 16s rrna sequencing stud-
760 ies. *Applied and Environmental Microbiology*, *81*(5), 1573-1584. Retrieved
761 from <https://journals.asm.org/doi/abs/10.1128/aem.02896-14> doi:
762 10.1128/AEM.02896-14
- 763 Peccoud, J., Lequime, S., Moltini-Conclois, I., Giraud, I., Lambrechts, L., &
764 Gilbert, C. (2018, 04). A survey of virus recombination uncovers canon-

- 767 ical features of artificial chimeras generated during deep sequencing li-
768 brary preparation. *G3 Genes—Genomes—Genetics*, 8(4), 1129-1138. Re-
769 trieved from <https://doi.org/10.1534/g3.117.300468> doi: 10.1534/
770 g3.117.300468
- 771 Qin, Y., Wu, L., Zhang, Q., Wen, C., Nostrand, J. D. V., Ning, D., ... Zhou, J.
772 (2023). Effects of error, chimera, bias, and gc content on the accuracy of
773 amplicon sequencing. *mSystems*, 8(6), e01025-23. Retrieved from <https://journals.asm.org/doi/abs/10.1128/msystems.01025-23> doi: 10.1128/
774 msystems.01025-23
- 775 Qiu, X., Wu, L., Huang, H., McDonel, P. E., Palumbo, A. V., Tiedje, J. M., &
776 Zhou, J. (2001). Evaluation of pcr-generated chimeras, mutations, and het-
777 eroduplexes with 16s rrna gene-based cloning. *Applied and Environmental
778 Microbiology*, 67(2), 880–887. doi: 10.1128/AEM.67.2.880-887.2001
- 780 Ren, J., Song, K., Deng, C., Ahlgren, N., Fuhrman, J., Li, Y., ... Sun, F. (2020,
781 01). Identifying viruses from metagenomic data using deep learning. *Quan-
782 titative Biology*, 8. doi: 10.1007/s40484-019-0187-4
- 783 Rodriguez-Martin, B., Palumbo, E., Marco-Sola, S., Griebel, T., Ribeca, P.,
784 Alonso, G., ... Djebali, S. (2017, 01). Chimpipe: Accurate detection of
785 fusion genes and transcription-induced chimeras from rna-seq data. *BMC
786 Genomics*, 18. doi: 10.1186/s12864-016-3404-9
- 787 Rognes, T., Flouri, T., Nichols, B., Quince, C., & Mahé, F. (2016). Vsearch: a
788 versatile open source tool for metagenomics. *PeerJ*, 4, e2584. doi: 10.7717/
789 peerj.2584
- 790 Sedlazeck, F., Rescheneder, P., Smolka, M., Fang, H., Nattestad, M., von Haeseler,
791 A., & Schatz, M. (2018, 06). Accurate detection of complex structural
792 variations using single-molecule sequencing. *Nature Methods*, 15. doi: 10

- 793 .1038/s41592-018-0001-7
- 794 795 796 797 798 Sfeir, A., & Symington, L. S. (2015). Microhomology-mediated end joining: A back-up survival mechanism or dedicated pathway? *Trends in Biochemical Sciences*, 40(11), 701-714. Retrieved from <https://www.sciencedirect.com/science/article/pii/S0968000415001589> doi: <https://doi.org/10.1016/j.tibs.2015.08.006>
- 799 800 801 802 803 Vervier, K., Mahé, P., Tournoud, M., Veyrieras, J.-B., & Vert, J.-P. (2015, 11). Large-scale machine learning for metagenomics sequence classification. *Bioinformatics*, 32(7), 1023-1032. Retrieved from <https://doi.org/10.1093/bioinformatics/btv683> doi: 10.1093/bioinformatics/btv683
- 804 805 806 Willette, D., Bognot, E., Mutia, M. T., & Santos, M. (2011). *Biology and ecology of sardines in the philippines: A review* (Vol. 13; Tech. Rep. No. 1). NFRDI Technical Paper Series. Retrieved from <https://nfrdi.da.gov.ph/tpjf/etc/Willette%20et%20al.%20Sardines%20Review.pdf>